

Current fed isolated DC/DC converter for future aerospace microgrids

Luca Tarisciotti*, Alessandro Costabeber, Linglin Chen, Adam Walker, Mikiel Galea
Department of Electrical and Electronics Engineering
University of Nottingham
Nottingham, UK
*ezzlt@nottingham.ac.uk

Abstract— High performance power conversion equipment is currently gaining an increasing interest for aircraft applications. In particular, isolated bidirectional DC/DC converters are often proposed for modern aircraft distribution systems. A current fed isolated DC/DC converter, named Active Clamp Active Bridge topology, is identified as the most promising for the proposed application, interfacing a 270V DC network with a 28V DC network. A comparison between the selected topology and the well-known Dual Active Bridge topology has been carried out and an experimental prototype has been manufactured for the selected conversion architecture. Simulation and experimental results are provided in order to validate the trade off and the design of the proposed converter.

Keywords—DC/DC power conversion, Power Electronics, Dual Active Bridge, Active Clamp Active Bridge, More Electric Aircraft

I. INTRODUCTION

In recent years, the More Electric Aircraft (MEA) concept has gained an increased importance [1]. In fact, electrical systems are replacing hydraulic, mechanical, or pneumatic power sources in a wide range of aerospace applications [2]. This increase in electrical energy demand has led to a rapid technology development, particularly in power electronics [3]. Electrical systems are now considered for aircraft actuation systems, wing ice protection systems, environmental control systems, and fuel pumping. These novel electrical systems aim to increase future aircraft efficiency, thus reducing the environmental impact of such systems and their maintenance cost. However, due to the electrical system complexity, future aircraft will face similar issues to the one found in ground based microgrids [1]–[3]. In such scenario, several structures for future aerospace microgrids have been proposed. Both AC and DC grids are investigated showing a trend in increasing the voltage level in such grids [4], [5]. Focusing on High Voltage Direct Current (HVDC) aerospace microgrids, Fig. 1 shows a typical grid structure which comprises a Low Voltage Direct Current (LVDC) network and a HVDC network. On the LVDC network typically Low Voltage (LV) emergency batteries and other energy storage elements, such as Electro-Mechanical Batteries (EMB) are connected together with the Electrical Power Unit (EPU) which supplies avionics circuitry [6]. On the HVDC network, High Voltage (HV) generators [7], [8] provide the required voltage and power, together with HV batteries [6] and other EPU [9], which supplies electric actuators, de-icing systems and other MEA equipment [10]–[12]. Moreover, Starter Generator (SG) systems [13], [14], together with their Electrical Control Unit (ECU) are able to provide the required power to

start the aircraft engines, and generate additional power during flight, on the HVDC or LVDC network.

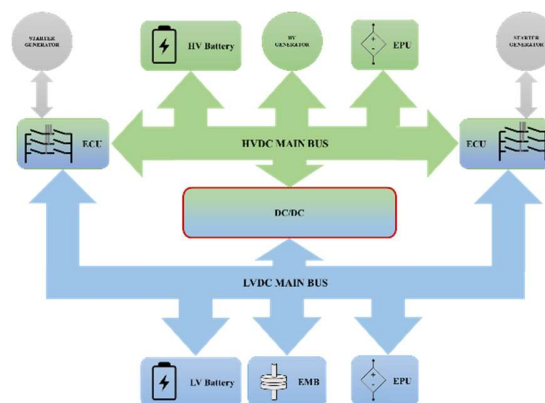


Fig. 1. Aircraft distribution network under investigation.

As shown in Fig.1, an isolated, bidirectional DC/DC converter has to be included in the system in order to provide an active interface between the two DC networks [15], [16]. The converter must be designed to provide high power density and high efficiency, to be integrated in the aircraft structure with minimum impact on volume, weight and heat management. At the same time, it must provide reliable and flexible operation, also capable to respond to fault events or other abnormal operating conditions with a controlled and predictable behaviour, while minimising the impact on power generation. In particular, the reliability of the DC-DC converter is crucial during “emergency flight” operation, as it will supply the essential equipment to guarantee flight safety. The converter will also operate in a stringent and harsh environment, including limited cooling capabilities; pressure drops, mechanical vibrations and possible EMC or lightning interference, and their operation should have minimum effect on the environment. In order to achieve these challenging requirements, it is clear that cutting-edge technological innovations and innovative design approaches will be required. Several isolated DC/DC converter topologies are proposed in literature. Flyback, Forward, and Forward-Flyback converters are investigated in [17], [18]. These topologies requires a minimal number of active devices, however, their low efficiency, compared with other converter structures limits their use in high power applications. Resonant converters, such as isolated LLC resonant DC/DC converter and Series Resonant (SR) converter [19] can also be considered for this application. They take advantage of resonant networks in order to achieve Zero Voltage Switching (ZVS) or Zero Current Switching (ZCS) commutations, providing highly efficient power conversion. However, additional passive components are

needed and control becomes challenging when a wide operating area is required by the application. On the other hand, Dual-Active-Bridge (DAB) [20] and Three-Phase Dual-Active-Bridge [21] present lower loss switching loss due to their natural capability of achieving ZVS commutation when the devices are turned on, in a wide operating range and without drastically increase the control system complexity. In unidirectional applications, Synchronous rectification also represents an high efficiency alternative to DAB [22]. However, it is not applicable to this work since bidirectional power flow is required. In alternative to DAB a current fed solution has been proposed in previous work, named Active Bridge Active Clamp (ABAC) converter [23]. In fact, the ABAC converter represent a promising solution for MEA applications, due to its inherent current control capabilities. In the following sections, the ABAC converter is introduced and compared with the DAB in terms of design, operating capabilities and weight and volume considerations. Simulations results are provided in several operating conditions in order to assess the benefits of ABAC converter. Experimental results are also provided on a 10kW prototype.

II. THE DUAL ACTIVE BRIDGE CONVERTER

The DAB converter [24], [25], shown in Fig. 2 is a well-known topology, which provides efficient DC/DC conversion as well as galvanic insulation.

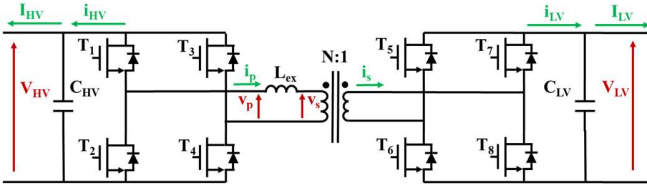


Fig. 2. The Dual Active Bridge (DAB) topology.

As shown in Fig. 2, the DAB consists of two H-Bridge linked on their AC sides with a series inductor and an HF transformer. Conventional Single Phase Shift (SPS) modulation scheme [26] is adopted. With SPS the duty cycle of each bridge/arm is kept constant at 50% of the sampling period, while the phase shift ϕ between the transformer primary and secondary voltage waveform is used to control the power transfer. Theoretical operation waveforms for such topology is drawn in Fig. 3, where V_p and V_s are transformer primary and secondary voltages, which operate at 50% duty cycle in SPS modulation, i_p is transformer primary current. i_{LV} and I_{LV} are the currents flowing before and after being filtered by the output capacitor C_{LV} . It is noted that the output current i_{LV} has considerably large ripple which needs a significantly large capacitive filter. The power transfer inductance L_{ex} on the primary side is designed in order to achieve the required power rating for the converter [20],

$$L_{ex} = \frac{NV_{HV}V_{LV}}{8f_s P_r} \quad (1)$$

where, N is transformer turn ratio, V_{HV} and V_{LV} are high DC bus voltage and low DC bus voltage respectively, f_s is switching frequency and P_{max} is the rated power. In order to design the filter capacitors, I_{p1} and I_{p2} in Fig. 3 can be calculated through following equations [20],

$$I_{p1} = \frac{1}{4f_s L_{ex}} (2V_{HV} \frac{\phi}{\pi} - V_{HV} + NV_{LV}) \quad (2)$$

$$I_{p2} = \frac{1}{4f_s L_{ex}} (2NV_{LV} \frac{\phi}{\pi} + V_{HV} - NV_{LV}) \quad (3)$$

Referring to Fig. 3, the time intervals Δ_1 and Δ_2 can be calculated using the following equations:

$$I_{p1} + \frac{V_{HV} - NV_{LV}}{L_{ex}} \Delta_1 = I_{p2} \rightarrow \Delta_1 = \frac{I_{p2} - I_{p1}}{V_{HV} - NV_{LV}} L_{ex} \quad (4)$$

$$I_{p2} - \frac{V_{HV} + NV_{LV}}{L_{ex}} \Delta_2 = \frac{I_{LV}}{N} \rightarrow \Delta_2 = \frac{I_{p2} - \frac{I_{LV}}{N}}{V_{HV} + NV_{LV}} L_{ex} \quad (5)$$

Therefore, the peak-to-peak output voltage ripple r_V can be obtained based on following equation:

$$r_V = \frac{\Delta V_{LV}}{V_{LV}} = \frac{\int_{t_1}^{t_1+\Delta_1+\Delta_2} (I_o - I_{LV}) dt}{V_{LV}} = \frac{Q_a + Q_b}{C_{LV} V_{LV}} \quad (6)$$

where,

$$Q_a = \frac{(NI_{p1} - I_{LV}) + (NI_{p2} - I_{LV})}{2} \Delta_1 \quad (7)$$

$$Q_b = \frac{(NI_{p2} - I_{LV})}{2} \Delta_2 \quad (8)$$

The output capacitor C_{LV} can then be derived from (6) as:

$$C_{LV} = \frac{Q_a + Q_b}{r_V V_{LV}} \quad (9)$$

A similar approach can be used to calculate the value of C_{HV} .

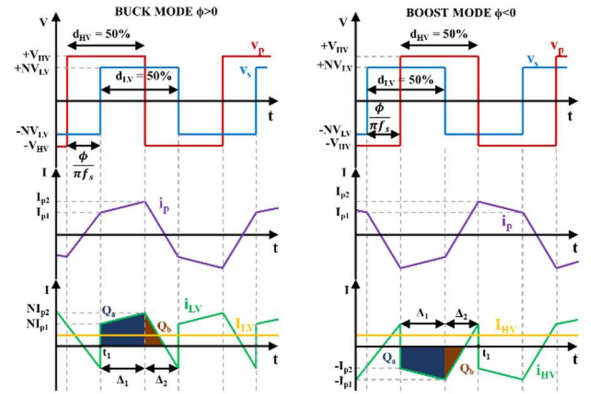


Fig. 3. Main waveforms for DAB with SPS modulation

In order to analyse the ZVS operating area for the DAB converter the voltage transfer ratio M is defined:

$$M = \frac{V_{LV}}{V_{HV}} \quad (10)$$

In buck operations, i.e. when the power is transferred from primary to secondary converter side, the secondary phase shift ϕ

is positive and ZVS is achieved when $I_{p1} > 0$ and $I_{p2} > 0$. Thus, from (2), (3) and (10) the following conditions can be obtained:

$$\frac{(1-NM)\pi}{2} < \phi < \frac{(NM-1)\pi}{2NM} \quad (11)$$

Similarly in boost operations, i.e. when the power is transferred from secondary to primary converter side, the secondary phase shift ϕ is negative and ZVS is achieved when $I_{p1} < 0$ and $I_{p2} < 0$, obtaining the following constraint:

$$\frac{(NM-1)\pi}{2NM} < \phi < \frac{(1-NM)\pi}{2} \quad (12)$$

In Fig. 4, the boundaries (11) and (12) are plotted for different values of N and the nominal operating conditions ($V_{HV} = 270V$ and $V_{LV} = 28V$) are highlighted. Results shows that when $N=10$, ZVS on switches turn-on can be achieved in almost the entire phase shift range for both primary and secondary switches.

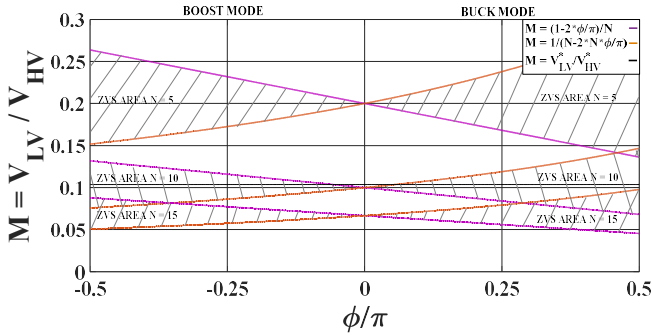


Fig. 4. Soft switching region for DAB.

The control scheme adopted with DAB converter is shown in Fig. 5 for both Buck mode, where the power flows from the HV network to a LV load, and Boost mode, where the power flows from the LV network to a HV load. Clearly only voltage control is feasible with DAB converter without adding additional inductors in the circuit. In terms of modulation, conventional Single Phase Shift (SPS) modulation is implemented. In this case the duty cycle of the HV and LV bridge, d_{HV} and d_{LV} respectively, are kept fixed at 50% of the sampling interval T_s . Implementation of SPS is straightforward but presents numerous disadvantages, such as large back-and-forth power [27], hard switching [20], [24], dead band effect [26] under light load non-nominal voltages operation condition. In order to overcome these problems, advanced modulations has been proposed in literature, such as Extended Phase Shift (EPS) [28], Dual Phase Shift (DPS) [29], Triple Phase Shift (TPS) [30], Triangular current Manipulation (TRM) and Trapezoidal current Manipulation (TZM) [31].

III. THE ACTIVE BRIDGE ACTIVE CLAMP CONVERTER

The ABAC converter, shown in Fig. 6, features a similar operating behaviour to the DAB. The main difference is that it provides a current-fed LV stage, taking advantage of external output inductors. The power transfer inductor L_{ex} transfers power from primary to the clamping circuits, while the two output inductors, L_1 and L_2 , serves as buffers to transfer energy from the clamping circuits to the LV output. When using SPS

modulation, the switches are all operating at 50% duty, and the two clamping circuits are complementarily switched in order to produce a square waveform on the transformer primary. The design of the input capacitor C_{HV} is identical to the one in DAB.

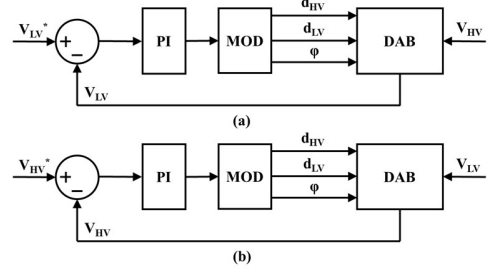


Fig. 5. Control block scheme for DAB converter: (a) Buck Mode (b) Boost Mode.

Similarly, the power transfer inductor L_{ex} can be designed in order to obtain the required power transfer:

$$L_{ex} = \frac{NV_{HV}v_{c1}}{8f_sP_r} = \frac{NV_{HV}v_{c2}}{8f_sP_r} \approx \frac{NV_{HV}V_{LV}}{4f_sP_r} \quad (13)$$

where N is the transformer turn ratio for the ABAC converter, and the voltage on the clamping capacitors v_{c1} and v_{c2} have an average value of twice the amplitude of V_{LV} when the converter is operating with SPS modulation and, thus, 50% of duty cycle. The main advantage of ABAC converter, with respect to DAB, is the capability of obtaining interleaved LV inductor currents i_{LV1} and i_{LV2} , resulting, ideally, in a purely DC current I_{LV} . Thus, there is no need of capacitive filtering on the LV side of the converter. However, a filter capacitance is used to suppress the current ripple related to converter asymmetries and load harmonics.

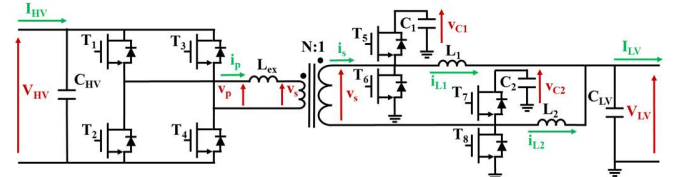


Fig. 6. The Active Bridge Active Clamp (ABAC) topology.

Assuming a desired current peak-to-peak ripple before the interleaved point is r_i , the constraint for the inductors L_1 and L_2 can be defined as:

$$\frac{2V_{LV}^2}{r_i f_s P_r} < L_1 = L_2 \quad (14)$$

Regarding ZVS turn-on operating region for the ABAC converter, the primary side boundary condition is derived as for DAB, considering that the clamp capacitor voltages v_{c1} and v_{c2} are approximately equal to twice the value of V_{LV}

$$M = \frac{v_{c1}}{V_{HV}} = \frac{v_{c2}}{V_{HV}} \approx \frac{2V_{LV}}{V_{HV}} \quad (15)$$

As for the DAB converter, the following soft switching constraint is obtained for the primary converter side in equations (16) and (17), for buck and boost operations, respectively.

$$\frac{(NM-1)\pi}{2NM} < \phi \quad (16)$$

$$\frac{(NM-1)\pi}{2NM} > \phi \quad (17)$$

On the other hand, ZVS constraint for secondary switches turn-on is defined referring to Fig. 7, where the hard turn-off of the switches already took place and, after the dead-time, the complimentary switch on each clamp circuits is turning on. It can be noted that in the case buck operations T5 and T8 are soft switched during turn-on only if the secondary current i_s is bigger than the respective inductor current. Vice-versa, in the case of boost operations, T6 and T7 are soft switched during turn-on only if the secondary current i_s is bigger than the respective inductor current, after inverting its sign.

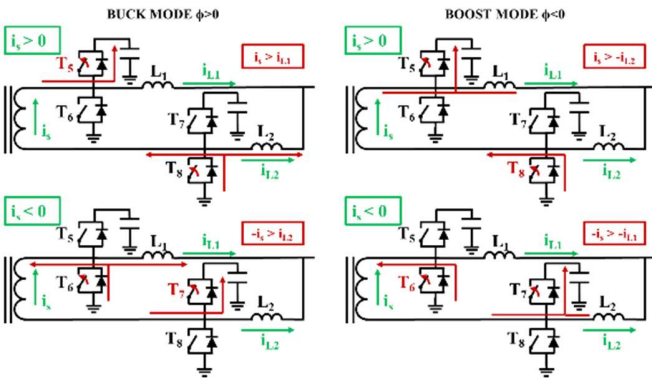


Fig. 7. Soft switching conditions for ABAC converter with SPS modulation

From Fig. 8 is possible to note that soft-switching conditions have to be satisfied when $i_{L1}/i_{L2} = \pm I_{Lmin}$ and $i_s = I_{s1}$.

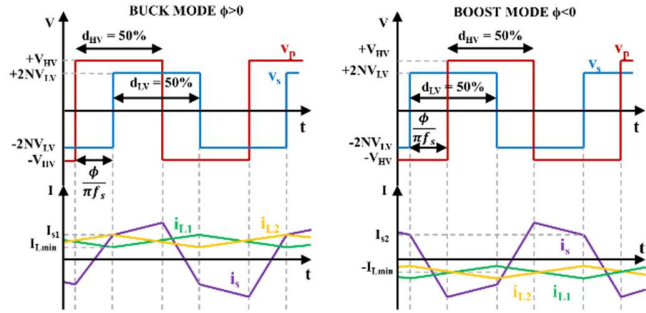


Fig. 8. Main waveforms for ABAC converter with SPS modulation

According to this analysis soft-switching conditions can be rewritten as in (18) and (19) for buck and boost operations, respectively.

$$I_{Lmin} < I_{s1} \quad (18)$$

$$I_{Lmin} < I_{s2} \quad (19)$$

The expressions of I_{Lmin} and I_{s1} are obtained as follows:

$$I_{Lmin} = \frac{NV_{HV}(\pi - \phi)\phi}{f_s L_{ex} \pi^2} - \frac{P_{max} r_l}{4V_{LV}} \quad (20)$$

$$I_{s1} = \frac{N}{4f_s L_{ex}} (2V_{HV} \frac{\phi}{\pi} - V_{HV} + 2NV_{LV}) \quad (21)$$

$$I_{s2} = \frac{N}{4f_s L_{ex}} (V_{HV} - 2V_{HV} \frac{\phi}{\pi} + 2NV_{LV}) \quad (22)$$

Equations (18) to (22) lead to complex expressions that can be simplified if a negligible current ripple r_l is considered for the output inductors, resulting in the soft-switching region expressed by equations (23) and (24) for buck and boost operations, respectively.

$$\sqrt{\frac{1-NM}{2}} \pi < \phi < \frac{(NM-1)\pi}{2NM} \quad (23)$$

$$\frac{(NM-1)\pi}{2NM} < \phi < \sqrt{\frac{NM-1}{2}} \pi \quad (24)$$

According to the condition in (23) and (24), where $r_l = 0$ is assumed, the ZVS region for ABAC converter is shown in Fig. 9 for various values of N.

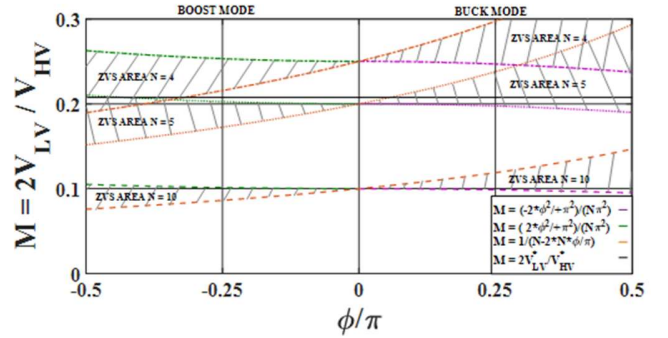


Fig. 9. Soft switching region for ABAC when $r_l=0$.

The results in Fig. 9 represent an ideal case where infinite output inductance is considered and, in terms of soft switching capabilities, represents the worst scenario. When a finite value of output inductance is considered, the increased value of r_l widens the soft switching are by adding an offset term to the boundary conditions, as shown in Fig. 10.

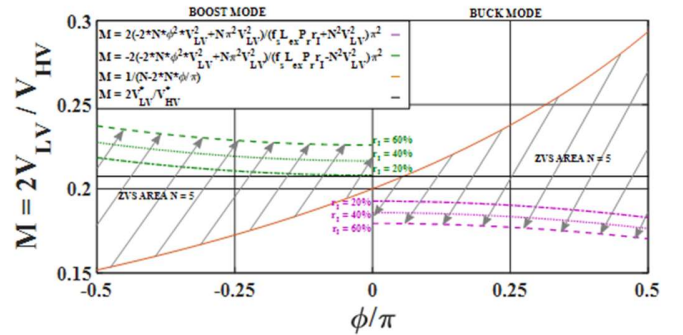


Fig. 10. Soft switching region for ABAC for $N=5$ and different values of output inductance.

In this general case the soft-switching region is expressed by equations (25) and (26) for buck and boost operations, respectively, with $L_0 = L_1 = L_2$ in Fig. 6.

selected for the converter LV side, while the C2M0025120D Silicon Carbide Mosfet, rated 1.2kV, 90A has been selected for the high voltage side. In order to perform a fair comparison the same number of devices in parallel has been selected for the two converters (one on the HV side and four on the LV side) with the only difference that for the ABAC converter these devices are equally divided between the two secondary circuits. Regarding the passive components, capacitors losses are considered negligible while only the DC losses are considered for the magnetics components. In fact, the AC losses can be minimized by performing an accurate planar magnetics design. The efficiency is estimated through PLECS simulations. The results, shown in Fig. 15, highlight the high efficiency for these two topologies when the soft switching constraints are satisfied. When the soft switching is lost as for example in the 300V/21V curve efficiency drops drastically due to increased switching losses. Advanced modulations can be implemented to increase the soft switching region. It is important to highlight that this efficiency analysis is carried out with the solely scope of comparing the two converter and do not represent an accurate measurement of efficiency, since additional losses in the magnetics are not considered and switches thermal models are obtained using datasheet parameters.

V. WEIGHT AND VOLUME CONSIDERATIONS

A first estimation of weight and volume for the three topologies has been calculated by considering off the shelf components and their datasheet information, shown in Table II, combined with the design parameters. The weight and volume estimation does not include heatsink weight and the additional weight and volume of PCB boards, wiring and other components. The design is carried out at three different power

rating, 5kW, 10kW and 20kW respectively, in order to identify trends in the components volume and weight. The results in Fig. 16, show that ABAC converter has more weight and volume associated with magnetic components while the DAB converter has an higher capacitor weight and volume.

TABLE II. SELECTED COMPONENTS

Components	Description	Weight [kg]	Volume [l]
LV Capacitor	Ceramic Capacitor, C Series, 1 μ F, 100V	0.0001	0.00036
LV Capacitor	Cornell Dubiler, Film Capacitor, 10 μ F, 50V	0.0007	0.0013
HV Capacitor	Film Capacitor, B32774 Series, 10 μ F, 450V	0.05	0.0116
5kW Transformer	STANDEX Series P350 series	0.4	0.0935
10kW Transformer	STANDEX Series P560 series	0.7	0.2513
20kW Transformer	STANDEX Series P900 series	1.2	0.6533
5kW Inductor	Micrometals E100-40 15.12 μ H@18Arms	0.0215	0.0096
5kW Inductor	Micrometals E100-2 1200nH@44Arms	0.027	0.0096
10kW Inductor	Micrometals E168-40 7.36 μ H@36Arms	0.0961	0.0628
10kW Inductor	Micrometals E160-2 600nH@88Arms	0.1065	0.0628
20kW Inductor	Micrometals E220-40 3.78 μ H@72Arms	0.2147	0.1296
20kW Inductor	Micrometals E220-2 300nH@176Arms	0.2235	0.1296
Output Inductor	Coilcraft SER3018H, 3.3 μ H, 93.6A	0.0364	0.0132
HV Device	CREE C2M0025120D, 90A, 1.2 kV	0.0011	0.0035
LV Device	INFINEON IPT020N10N3, 300A, 100 V	0.0014	0.0003

The increased capacitor weight and volume in DAB is mainly related to their demanding current capabilities which requires a combination of film and ceramic capacitors and discourage the use of electrolytic capacitors. On the other hand even if magnetics in the ABAC converter has to handle high currents, their inductance value is relatively low and few turns are required, thus reducing their weight and volume and allowing further optimization of these components. This trend gets more and more evident when increasing the rated power, making the ABAC converter particularly suitable for high power ratings.

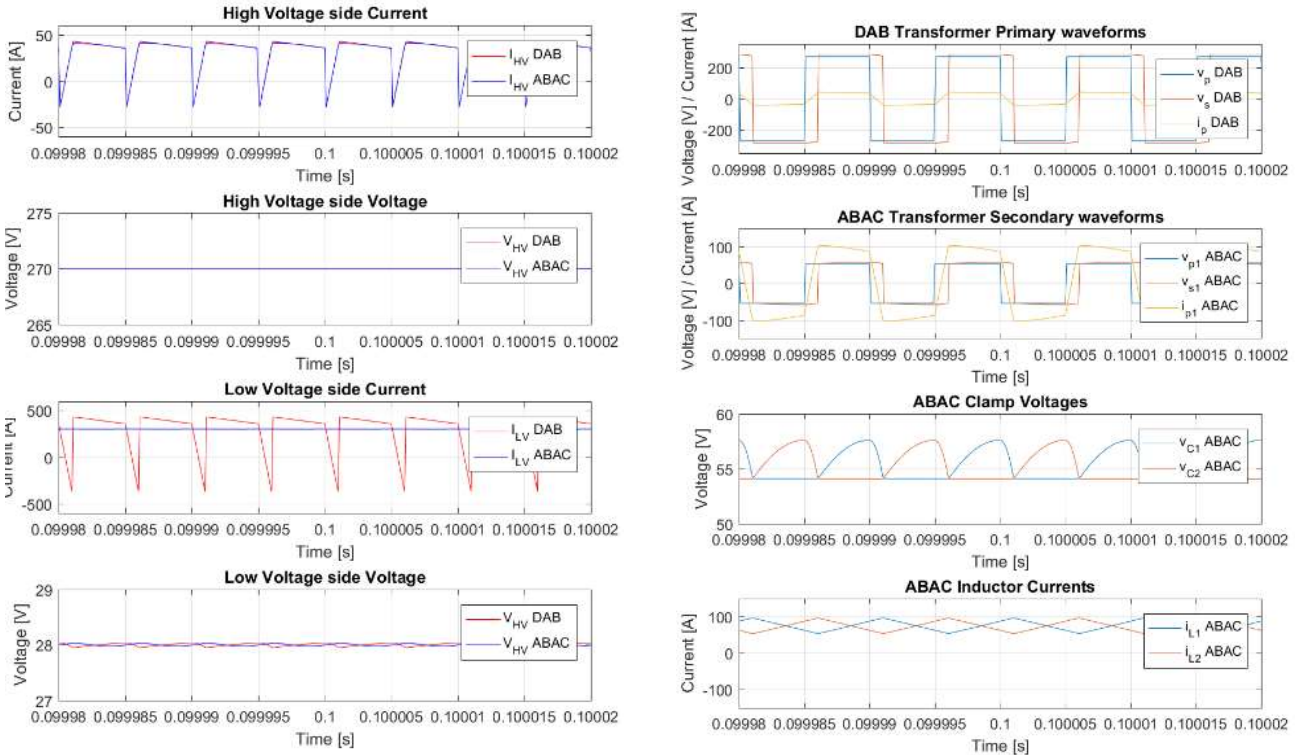


Fig. 13. Simulation results: Waveforms in Buck mode operation for DAB and ABAC converter when transferring 8.4kW on a resistive LV load.

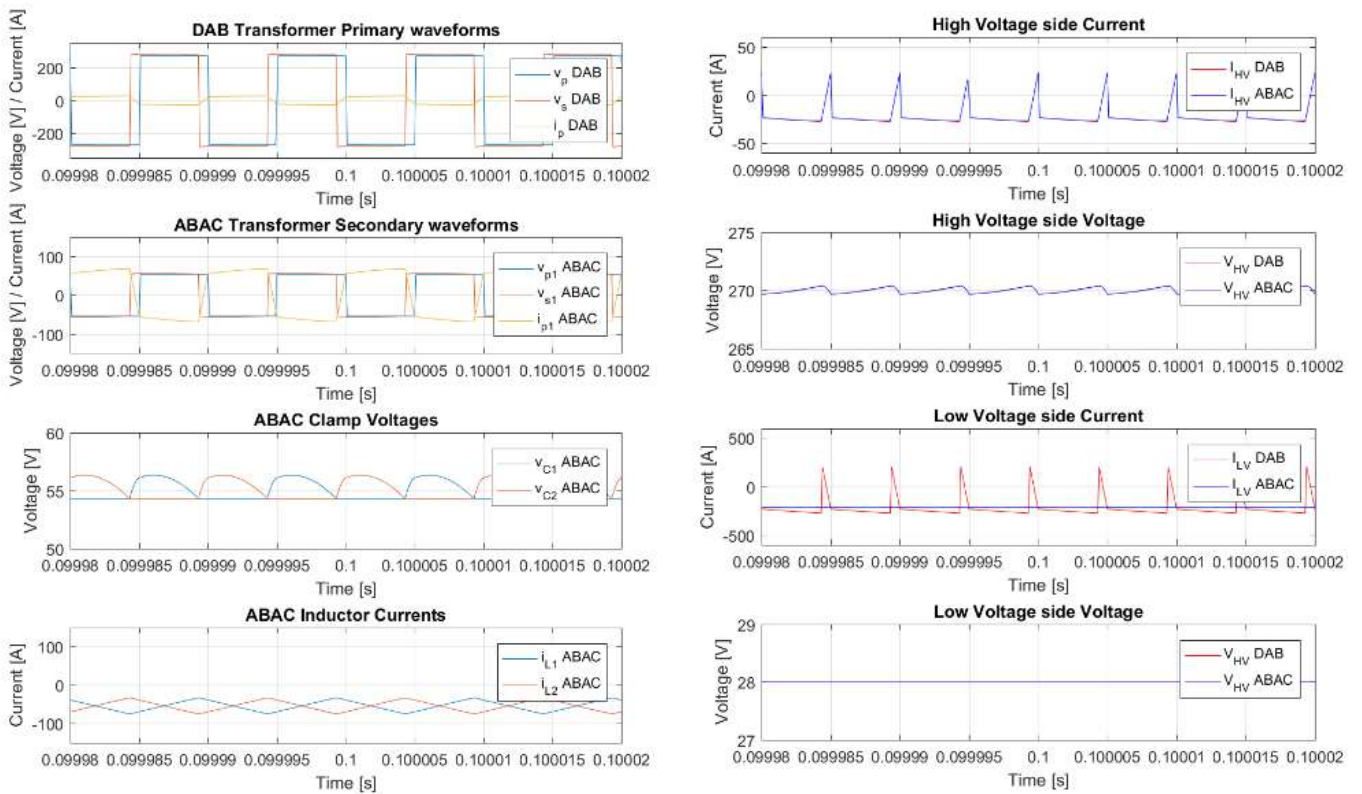


Fig. 14. Simulation results: Waveforms in Boost mode operation for DAB and ABAC converter when transferring 6kW on a resistive HV load;

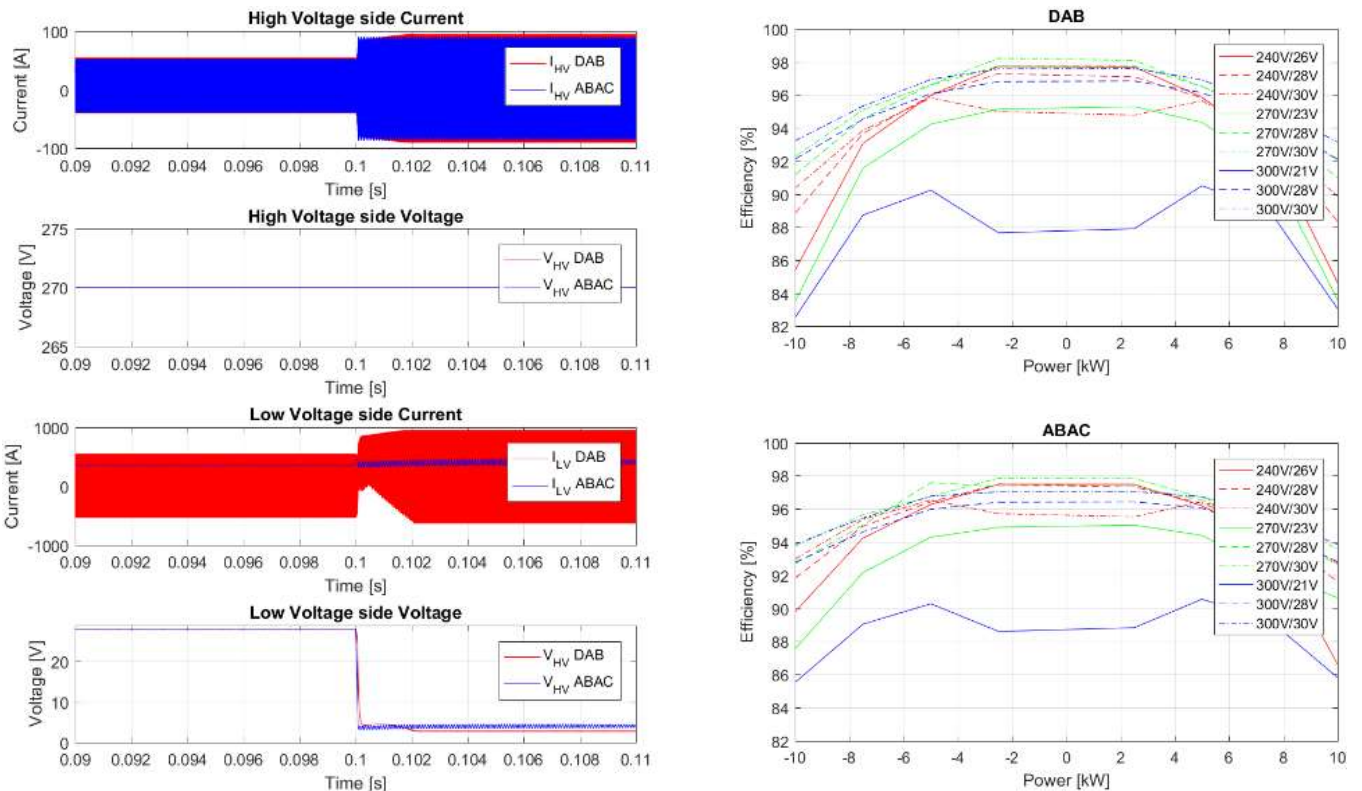


Fig. 15. Simulation results: Waveforms during Buck mode operations when transferring 10kW on a resistive LV load and imposing a short circuit on the load at time 0.1s with short circuit resistance of 78.4 mΩ; Efficiency estimation in various operating conditions for both DAB and ABAC converter.

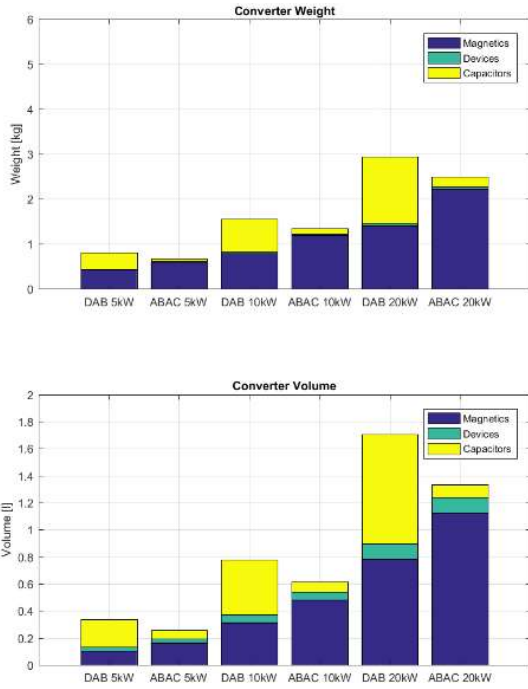


Fig. 16. Weight and volume estimation for the topologies under investigation.

VI. EXPERIMENTAL RESULTS

A 8.4kW experimental prototype based on the ABAC converter has been manufactured, as shown in Fig. 17. Experimental results are shown in Fig. 18 and Fig.19 when the converter is operating in buck and boost mode, respectively.

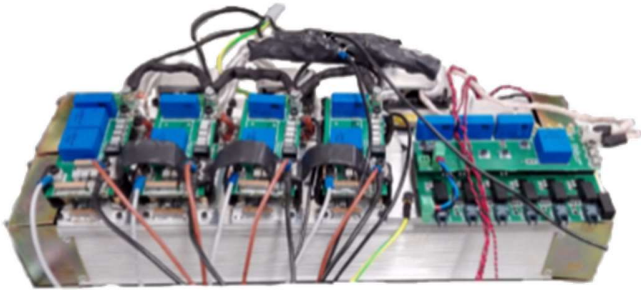


Fig. 17. ABAC Converter prototype.

The results are obtained considering the design parameters of Table I and a power transferred to the load of 3kW and 5kW, in buck and boost mode respectively. Voltages and currents at primary and one secondary of the HF transformer are presented, as well as voltage and current on both converter external interfaces (supply and load). The load voltage is well regulated at 28V, while providing the load current without any noticeable oscillation. On the other hand, looking at the current flowing through one of the four output inductors, it is possible to notice that the triangular ripple, which is cancelled at the load point, matches the value previously obtained in simulations. Experimental results validate the results of simulations except for the inductive voltage drops on the secondary transformer voltage, which are caused from parasitic inductance on the PCB board design.

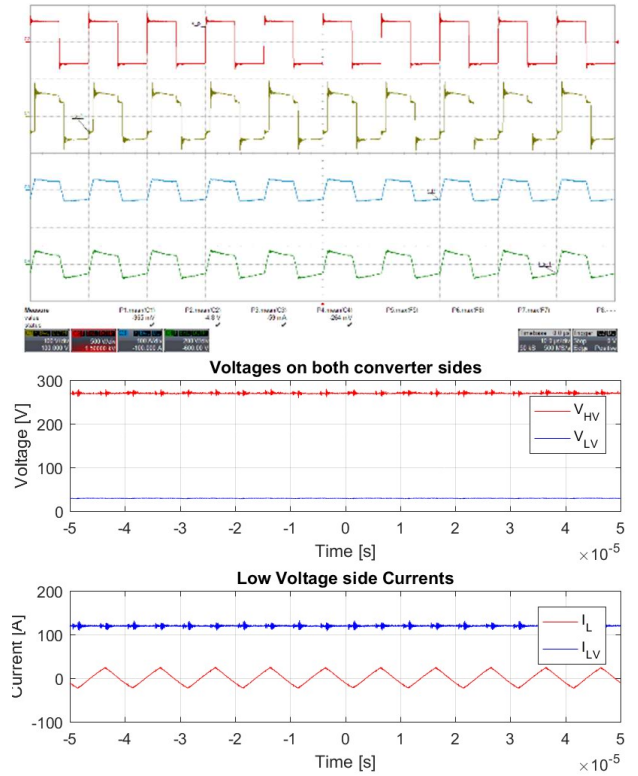


Fig. 18. Experimental results for the proposed ABAC topology in buck mode. v_p (red, 500V/div), v_{s1} (yellow, 100V/div), i_p (blue, 50A/div), i_{s1} (green, 100A/div); Voltage and current on HV and LV converter side, Inductor current.

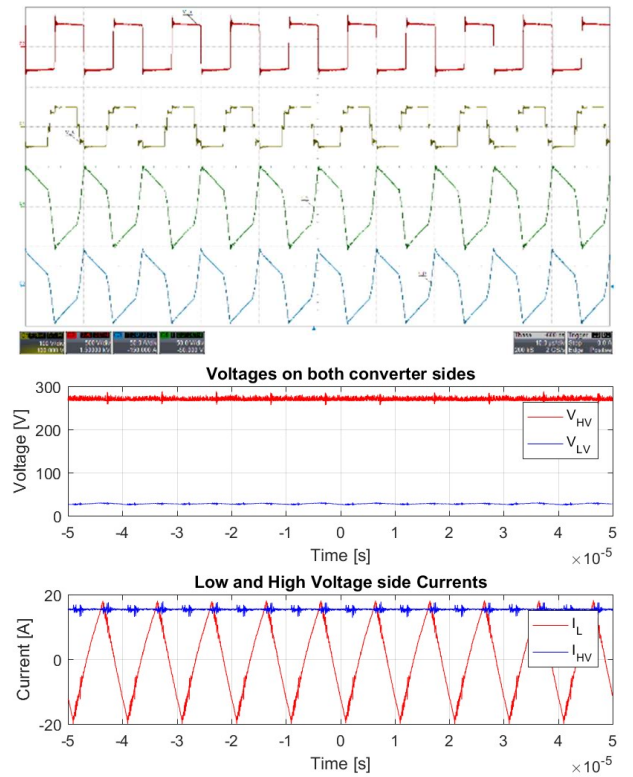


Fig. 19. Experimental results for the proposed ABAC topology in boost mode. v_p (red, 500V/div), v_{s1} (yellow, 100V/div), i_p (blue, 50A/div), i_{s1} (green, 100A/div); Voltage and current on HV and LV converter side, Inductor current.

VII. CONCLUSIONS

In this work a comparison between DAB converter and ABAC converter for aerospace applications has been carried out. The two topologies are compared in terms efficiency, weight and volume for the specific application of a 270V/28V 10kW bidirectional DC/DC converter. The design procedure has been described and soft switching analysis has been performed for both topologies. Accordingly to these analysis the two converter are evaluated through simulations in term to input and output waveforms, control, and efficiency. Additionally a first estimation of weight and volume for the two topologies when the converter power rating vary from 5kW to 20kW is carried out. Finally, experimental results validate the results obtained by simulations. From the obtained results it can be concluded that the ABAC converter represents a promising alternative to the DAB converter, able to reduce the converter weight and volume at high power ratings and inherently control the LV current whilst maintaining similar efficiency of a DAB converter.

REFERENCES

- [1] P. Wheeler and S. Bozhko, "The More Electric Aircraft," *IEEE Electr. Mag.*, vol. 2, no. 4, pp. 6–12, 2014.
- [2] B. Sarlioglu and C. T. Morris, "More Electric Aircraft: Review, Challenges, and Opportunities for Commercial Transport Aircraft," *IEEE Trans. Transp. Electr.*, vol. 1, no. 1, pp. 54–64, 2015.
- [3] P. Wheeler, "Technology for the More and All Electric Aircraft of the Future," *IEEE Int. Conf. Autom.*, 2016.
- [4] K. Areerak, S. V. Bozhko, G. M. Asher, L. De Lillo, and D. W. P. Thomas, "Stability Study for a Hybrid AC-DC More-Electric Aircraft Power System," *IEEE Trans. Aerosp. Electron. Syst.*, vol. 48, no. 1, pp. 329–347, 2012.
- [5] I. Christou, A. Nelms, I. Cotton, and M. Husband, "Choice of optimal voltage for more electric aircraft wiring systems," *IET Electr. Syst. Transp.*, vol. 1, no. 1, pp. 24–30, 2011.
- [6] M. Tariq, A. I. Maswood, C. J. Gajanayake, and A. K. Gupta, "Aircraft batteries: current trend towards more electric aircraft," *IET Electr. Syst. Transp.*, vol. 7, no. 2, pp. 93–103, 2017.
- [7] M. Hirst, A. McLoughlin, P. J. Norman, and S. J. Galloway, "Demonstrating the more electric engine: a step towards the power optimised aircraft," *IET Electr. Power Appl.*, vol. 5, no. 1, pp. 3–13, 2011.
- [8] E. Ganev, "Selecting the best electric machines for electrical power-generation systems: High-performance solutions for aerospace More electric architectures," *IEEE Electr. Mag.*, vol. 2, no. 4, pp. 13–22, 2014.
- [9] W. Rohouma, P. Zanchetta, P. W. Wheeler, and L. Empringham, "A Four-Leg Matrix Converter Ground Power Unit With Repetitive Voltage Control," *IEEE Trans. Ind. Electron.*, vol. 62, no. 4, pp. 2032–2040, 2015.
- [10] A. Trentin, P. Zanchetta, P. Wheeler, and J. Clare, "Power flow analysis in electro-mechanical actuators for civil aircraft," *IET Electr. Power Appl.*, vol. 5, no. 1, p. 48, 2011.
- [11] M. Villani, M. Tursini, G. Fabri, and L. Castellini, "Electromechanical Actuator for Helicopter Rotor Damper Application," *IEEE Trans. Ind. Appl.*, vol. 50, no. 2, pp. 1007–1014, 2014.
- [12] A. Nothofer, L. Tarisciotti, Q. Zhou, T. Benson, S. Greedy, and C. Christopoulos, "Analysis of conducted emissions from an Electric Nacelle Anti-Ice Power Control System," *Int. Symp. Electromagn. Compat. - EMC Eur.*, pp. 434–439, 2016.
- [13] L. Chédot, G. Friedrich, J. Biedinger, and P. Macret, "Integrated Starter Generator: The Need for an Optimal Design and Control Approach. Application to a Permanent Magnet Machine," *IEEE Trans. Ind. Appl.*, vol. 43, no. 2, pp. 551–559, 2007.
- [14] G. Friedrich and A. Girardin, "Integrated starter generator," *IEEE Ind. Appl. Mag.*, vol. 15, no. 4, pp. 26–34, 2009.
- [15] S. Pugliese, R. A. Mastromauro, and S. Stasi, "270V/28V Wide Bandgap Device-Based DAB Converter for More-Electric-Aircrafts: feasibility and optimization," *Electr. Syst. Aircraft, Railw. Sh. Propuls.*, 2016.
- [16] D. Izquierdo, R. Azcona, F. J. L. del Cerro, C. Fernández, and B. Delicado, "Electrical Power Distribution System (HV270DC), for Application in More Electric Aircraft," *IEEE Appl. Power Electron. Conf. Expo.*, no. 1, pp. 1300–1305, 2010.
- [17] A. Connaughton, A. P. Talei, K. K. Leong, K. Krischan, and A. Muetze, "Investigation of a Soft-Switching Flyback Converter With Full Secondary Side-Based Control," *IEEE Trans. Ind. Appl.*, vol. 53, no. 6, pp. 5587–5601, 2017.
- [18] M. Forouzes, Y. P. Siwakoti, S. A. Gorji, F. Blaabjerg, and B. Lehman, "Step-Up DC–DC Converters: A Comprehensive Review of Voltage-Boosting Techniques, Topologies, and Applications," *IEEE Trans. Power Electron.*, vol. 32, no. 12, pp. 9143–9178, 2017.
- [19] A. Chub, D. Vinnikov, F. Blaabjerg, and F. Z. Peng, "A Review of Galvanically Isolated Impedance-Source DC–DC Converters," *IEEE Trans. Power Electron.*, vol. 31, no. 4, pp. 2808–2828, 2016.
- [20] A. R. Alonso, J. Sebastian, D. G. Lamar, M. M. Hernandez, and A. Vazquez, "An overall study of a Dual Active Bridge for bidirectional DC/DC conversion," *2010 IEEE Energy Conversion Congress and Exposition*, pp. 1129–1135, 2010.
- [21] R. De Doncker, D. M. Divan, and M. H. Kheraluwala, "A three-phase soft-switched high-power-density DC/DC converter for high-power applications," *IEEE Trans. Ind. Appl.*, vol. 27, no. 1, pp. 63–73, 1991.
- [22] U. Badstuebner, J. Biela, and J. W. Kolar, "An optimized, 99% efficient, 5 kW, phase-shift PWM DC-DC converter for data centers and telecom applications," in *The 2010 International Power Electronics Conference - ECCE ASIA -*, 2010, pp. 626–634.
- [23] L. Tarisciotti, A. Costabeber, C. Linglin, A. Walker, and M. Galea, "Evaluation of isolated DC/DC converter topologies for future HVDC aerospace microgrids," *IEEE Energy Convers. Congr. Expo.*, pp. 2238–2245, 2017.
- [24] M. H. Kheraluwala, R. W. Gascoigne, D. M. Divan, and E. D. Baumann, "Performance characterization of a high-power dual active bridge DC-to-DC converter," *IEEE Trans. Ind. Appl.*, vol. 28, no. 6, pp. 1294–1301, 1992.
- [25] F. Krismer and J. W. Kolar, "Accurate Small-Signal Model for the Digital Control of an Automotive Bidirectional Dual Active Bridge," *IEEE Trans. Power Electron.*, vol. 24, no. 12, pp. 2756–2768, 2009.
- [26] H. Bai, C. C. Mi, and S. Gargies, "The Short-Time-Scale Transient Processes in High-Voltage and High-Power Isolated Bidirectional DC-DC Converters," *IEEE Transactions on Power Electronics*, vol. 23, no. 6, pp. 2648–2656, 2008.
- [27] B. Zhao, Q. Song, W. Liu, G. Liu, and Y. Zhao, "Universal High-Frequency-Link Characterization and Practical Fundamental-Optimal Strategy for Dual-Active-Bridge DC-DC Converter Under PWM Plus Phase-Shift Control," *IEEE Trans. Power Electron.*, vol. 30, no. 12, pp. 6488–6494, Dec. 2015.
- [28] G. G. Oggier, G. O. García, and A. R. Oliva, "Switching Control Strategy to Minimize Dual Active Bridge Converter Losses," *IEEE Trans. Power Electron.*, vol. 24, no. 7, pp. 1826–1838, Jul. 2009.
- [29] Hua Bai and C. Mi, "Eliminate Reactive Power and Increase System Efficiency of Isolated Bidirectional Dual-Active-Bridge DC–DC Converters Using Novel Dual-Phase-Shift Control," *IEEE Trans. Power Electron.*, vol. 23, no. 6, pp. 2905–2914, Nov. 2008.
- [30] Y. A. Harrye, K. . Ahmed, G. . Adam, and A. . Aboushady, "Comprehensive steady state analysis of bidirectional dual active bridge DC/DC converter using triple phase shift control," in *2014 IEEE 23rd International Symposium on Industrial Electronics (ISIE)*, 2014, pp. 437–442.
- [31] G. Xu, D. Sha, J. Zhang, and X. Liao, "Unified Boundary Trapezoidal Modulation Control Utilizing Fixed Duty Cycle Compensation and Magnetizing Current Design for Dual Active Bridge DC–DC Converter," *IEEE Trans. Power Electron.*, vol. 32, no. 3, pp. 2243–2252, Mar. 2017.
- [32] Y. Shi, R. Li, Y. Xue, and H. Li, "Optimized Operation of Current-Fed Dual Active Bridge DC-DC Converter for PV applications," *IEEE Trans. Ind. Electron.*, vol. 62, no. 11, pp. 6986–6995, 2015.

- [33] Z. Guo, K. Sun, T.-F. Wu, and canbing Li, "An Improved Modulation Scheme of Current-fed Bidirectional DC-DC Converters for Loss Reduction," *IEEE Trans. Power Electron.*, pp. 1–1, 2017.
- [34] L. Chen, L. Tarisciotti, A. Costabeber, P. Zanchetta, and P. Wheeler, "Advanced modulation for the Active-Bridge-Active-Clamp (ABAC) converter," *IEEE South. Power Electron. Conf.*, pp. 1–6, 2017.



Luca Tarisciotti (S'12-M'15) received the Master's degree in Electronic Engineering from The University of Rome "Tor Vergata" in 2009 and his Ph.D. degree in Electrical and Electronic Engineering from the PEMC group, University of Nottingham in 2015. In the same year he started working as Research Fellow at the University of Nottingham, UK until 2018. He is currently working as Adjunct Professor at the University of Chile, Santiago, Chile. His research interests includes Matrix converters, DC/DC converters, Multilevel converters, Advanced modulation schemes, and Advanced power converter control.



Alessandro Costabeber (S'09 - M'13) received the Degree with honours in Electronic Engineering from the University of Padova, Padova, Italy, in 2008 and the Ph.D. in Information Engineering from the same university in 2012, on energy efficient architectures and control techniques for the development of future residential microgrids. In the same year he started a two-year research fellowship with the same university. In 2014 he joined the PEMC group, Department of Electrical and Electronic Engineering, University of Nottingham, Nottingham, UK as Lecturer in Power Electronics. His current research interests include HVDC converters topologies, high power density converters for aerospace applications, control solutions and stability analysis of AC and DC microgrids, control and modelling of power converters, power electronics and control for distributed and renewable energy sources. Dr. Costabeber received the IEEE Joseph John Suozzi INTELEC Fellowship Award in Power Electronics in 2011.



Linglin Chen received his MSc degree in Electrical Engineering from Zhejiang University, Hangzhou, China, in 2016 on construction of a demonstrative high reliability microgrid. He is currently with the PEMC group in the University of Nottingham, U.K. as a Ph.D. candidate. His current research interests include isolated DC/DC power converters, advanced modulation schemes, nonlinear power converter controls and stability of microgrids in more electric aircraft.

- [35] L. Chen, L. Tarisciotti, A. Costabeber, P. Zanchetta, and P. Wheeler, "Parameters mismatch analysis for the Active-Bridge-Active-Clamp (ABAC) converter," *IEEE South. Power Electron. Conf.*, pp. 1–6, 2017.



Adam Walker (M'18) received his PhD in electrical machines design from the University of Nottingham, UK, in 2016, where he has also worked as a Research Associate. He is currently an Assistant Professor of Electrical Machines and Drives with the Power Electronics Machines and Control group at the University of Nottingham. His main research area is electrical machines for traction applications, both personal vehicle and heavy duty vehicles, but is also interested in thermal management of machines and design of passive magnetic components.



Michael Galea (M'13-SM'18, FRAeS) received his PhD in electrical machines design from the University of Nottingham, UK, where he has also worked as a Research Fellow. He is currently the Head of School of Aerospace in the University of Nottingham, Ningbo, China, where he is also the Director of Aerospace. He currently lectures in Electrical Drives and in Aerospace Systems Integration and manages a number of diverse projects and programmes related to the more / all electric aircraft, electrified propulsion and associated fields. His main research interests are design, analysis and thermal management of electrical machines and drives (classical and unconventional), the more electric aircraft and electrified and hybrid propulsion. He is a Fellow of the Royal Aeronautical Society and a Senior Member of the IEEE.